



## In situ exsolved Co nanoparticles on Ruddlesden-Popper material as highly active catalyst for CO<sub>2</sub> electrolysis to CO

Seongmin Park<sup>a</sup>, Yoongon Kim<sup>b</sup>, Hyunsu Han<sup>a</sup>, Yong Sik Chung<sup>a</sup>, Wongun Yoon<sup>a</sup>, Junil Choi<sup>a</sup>, Won Bae Kim<sup>a,\*</sup>

<sup>a</sup> Department of Chemical Engineering, Pohang University of Science and Technology (POSTECH), Pohang 37673, Republic of Korea

<sup>b</sup> School of Materials Science & Engineering, Gwangju Institute of Science and Technology (GIST), Gwangju 61005, Republic of Korea



### ARTICLE INFO

#### Keywords:

Solid oxide electrolysis cell (SOEC)  
CO<sub>2</sub> reduction  
Exsolution of Co nanoparticles  
Ceramic cathode  
Ruddlesden-Popper structure

### ABSTRACT

We report a highly active Ruddlesden-Popper material with a mechanism of in situ exsolution of Co nanoparticles and its use as an effective catalyst for CO<sub>2</sub> reduction to produce CO in a solid oxide electrolysis cell. This catalyst is simply prepared by transforming a perovskite of La<sub>0.6</sub>Sr<sub>0.4</sub>Co<sub>0.7</sub>Mn<sub>0.3</sub>O<sub>3</sub> and revealed a good reversibility of structural transition between the Ruddlesden-Popper and the perovskite structure during reaction cycles. A very high current density of 630 mA/cm<sup>2</sup> can be accomplished at a voltage of 1.3 V and temperature of 850 °C with a very high Faraday efficiency of 95% or larger. More importantly, no sign of degradation is indicated as observed by galvanostatic stability test, implying that this Ruddlesden-Popper structure is highly robust as the cathode catalyst for the CO<sub>2</sub> electrolysis. In situ exsolved Co nanoparticles and high concentration of oxygen vacancies caused by the structural transition are responsible for its high stability and catalytic activity, as characterized by several physicochemical analyses.

### 1. Introduction

The concentration of CO<sub>2</sub> in the atmosphere has been steadily increasing as the use of fossil fuels increases, which makes greenhouse gas effect as the main causative factor of climate change and environment concerns. Currently, electrochemical conversion of CO<sub>2</sub> into various chemical species has been evaluated for CO<sub>2</sub> utilization and recycling. Solid oxide electrolysis cell (SOEC) may provide an effective CO<sub>2</sub> conversion approach by electrolyzing CO<sub>2</sub> to CO with several technological advantages such as fast electrode kinetics, high efficiency and decreased load of electrical energy compared to other methods [1–5]. However, several problems related to the cathode process of SOEC like carbon deposition, low stability and severe degradation must be solved [6–10].

Recent research has focused on finding new and effective cathode catalyst material to replace the conventional Ni-YSZ for high temperature CO<sub>2</sub> electrolysis. Ni-based cathode catalysts possess outstanding electrical conductivity and catalytic activity for the electrolysis reaction, but it has fatal drawbacks of serious degradation due to carbon deposition and loss of electrical conductivity caused by partial oxidation of Ni [11–15]. Ceramic-based materials in forms of perovskites are considered promising candidates for the cathode catalysts of SOEC because of their high stability under electrochemical redox

condition and coking resistance despite their relatively low catalytic activity [3]. Therefore, many studies have made efforts to improve the catalytic activity of ceramic-based material for the electrolysis process as compared with metal based catalysts such as Ni.

For the enhanced catalytic activity of such ceramic-based catalyst materials, impregnating some catalytically active metal nanoparticles such as Ni, Co, Fe and Cu on the cathode materials has been attempted [16–20], which is of a straightforward strategy to improve the catalytic activity of electrode by directly incorporating the active catalyst nanoparticles. However, cell degradation caused by coalescence and agglomeration of the small metal nanoparticles is serious issue that is not easy to solve. Alternatively, it is found that in situ growth of metal nanoparticles from parent ceramic materials could generate more-uniformly distributed metal nanoparticles than those from the impregnation method, allowing to minimize the coalescence and agglomeration of metal nanoparticles under operating temperature [21–26]. Indeed, SOECs that employ a cathode catalyst material of in situ exsolved metal nanoparticles have been reported to show high catalytic activity together with excellent stability during CO<sub>2</sub> electrolysis at high temperature [27,28].

The Ruddlesden-Popper structure (A<sub>2</sub>BO<sub>4</sub>), also called K<sub>2</sub>NiF<sub>4</sub> structure as a representative one, has been developed as both of anode

\* Corresponding author.

E-mail address: [kimwb@postech.ac.kr](mailto:kimwb@postech.ac.kr) (W.B. Kim).

and cathode materials for solid oxide cells (SOEC and SOFC) [29–31]. This structure is applicable to the solid oxide cell electrodes because it has good  $O^{2-}$  ion conductivity with fast surface oxygen exchange and high redox stability [32–34]. A catalyst composed of Ruddlesden-Popper structured ceramic parent with in situ exsolved Fe nanoparticles was reported previously as the anode catalyst material for solid oxide fuel cell (SOFC) [29]. However, high calcination temperature around 1350 °C is required for direct synthesis of the Ruddlesden-Popper structure.

Herein, we demonstrate an  $La_{1.2}Sr_{0.8}Co_{0.4}Mn_{0.6}O_4$  that has Ruddlesden-Popper structure (denoted as ‘R.P.LSCoMn’; the ceramic support part of Co-R.P.LSCoMn) and contains in situ exsolved Co metal nanoparticles (denoted as ‘Co-R.P.LSCoMn’) as an effective cathode catalyst material for  $CO_2$  electrolysis. The catalyst was synthesized by directly reducing a perovskite-derivative of  $La_{0.6}Sr_{0.4}Co_{0.7}Mn_{0.3}O_3$  (denoted as ‘LSCoMn’) in a reducing gas of 20%  $H_2/N_2$  at 800 °C, which is a much milder condition than the typical preparation methods of Ruddlesden-Popper structure. The structural and chemical properties of catalyst were characterized by means of X-ray diffraction (XRD), scanning electron microscopy (SEM), transmission electron microscopy (TEM), energy-dispersive X-ray spectrometry (EDS), X-ray absorption near-edge spectroscopy (XANES), thermogravimetric analysis (TGA),  $H_2$ -temperature programmed reduction ( $H_2$ -TPR),  $O_2$ -temperature programmed oxidation ( $O_2$ -TPO) and  $CO_2$ -temperature programmed desorption ( $CO_2$ -TPD). Moreover, electrochemical catalytic activity and Faraday efficiency of this novel cathode catalyst were quantified to evaluate its suitability as the cathode material in an SOEC.

## 2. Experimental procedure

### 2.1. Catalyst preparation

The perovskite  $La_{0.6}Sr_{0.4}Co_{0.7}Mn_{0.3}O_3$  (LSCoMn) was synthesized using a sol-gel method from metal precursors of  $La(NO_3)_3 \cdot 6H_2O$  (99.9%, Sigma Aldrich),  $Sr(NO_3)_2$  (99.0%, Sigma Aldrich),  $Co(NO_3)_2 \cdot 6H_2O$  (99.0%, Sigma Aldrich),  $Mn(NO_3)_2 \cdot 6H_2O$  (98 + %, Alfa Aesar) which were dissolved at stoichiometric ratios in distilled water. The precursor solution was stirred sufficiently, then ethylenediamine tetraacetic acid (EDTA, 99.5%, Sigma Aldrich) and citric acid (99.5%, Daejung, Korea) were introduced as chelating materials, with the molar ratio of metal ions/citric acid/EDTA to 1:1.5:1. Afterward, the pH of the solution was adjusted to 7 by adding ammonia water (28–30%, SAMCHUN) and the solution was stirred at 90 °C until the solution was gelled. The gel was dried at 200 °C for 1 h under air, then preheated at 700 °C for 10 h to eliminate the organic components. The sample was pulverized using a mortar, then calcined at 1100 °C for 10 h in air to obtain black powder. The  $La_{1.2}Sr_{0.8}Co_{0.4}Mn_{0.6}O_4$  (R.P.LSCoMn), the support part of Co-R.P.LSCoMn, was also synthesized by the same process using a sol-gel method except for the applied calcination temperature (1350 °C). The same metal precursors of  $La(NO_3)_3 \cdot 6H_2O$ ,  $Sr(NO_3)_2$ ,  $Co(NO_3)_2 \cdot 6H_2O$  and  $Mn(NO_3)_2 \cdot 6H_2O$  in the stoichiometric ratio were dissolved in distilled water. The precursor solution was stirred sufficiently, then citric acid and EDTA were introduced at the molar ratio of metal ions/citric acid/EDTA to 1:1.5:1. While stirring, the pH of the solution was adjusted to 7 by addition of ammonia water and then heated for evaporation of water at 90 °C to form a gel. The gel was dried at 200 °C for 1 h, then preheated at 700 °C for 10 h to remove organic residue. The sample was ground using a mortar, then calcined at 1350 °C for 10 h in air to obtain black powder of R.P.LSCoMn. Co impregnated R.P.LSCoMn catalyst, in which the same amount of Co was loaded as the amount of exsolved Co in the Co-R.P.LSCoMn, was prepared by adding drops of aqueous  $Co(NO_3)_2 \cdot 6H_2O$  solution onto the R.P.LSCoMn and dried at 200 °C for 1 h. The powder was calcined at 1000 °C for 1 h to form cobalt oxide. Finally, prior to test the cell with the sample, 20%  $H_2/N_2$  reducing gas at a flow rate of 50 sccm was fed into the cathode for 0.5 h to induce reduction of cobalt oxide to cobalt metal.  $LaCoO_3$  and  $LaMnO_3$  were also synthesized by the same sol-gel method.

### 2.2. Electrolyte-electrode fabrication

The single cell test was conducted with an electrolyte-supported button cell. A portion of electrolyte powder,  $La_{0.8}Sr_{0.2}Ga_{0.8}Mg_{0.2}O_3$  (LSGM, Fuel cell materials), was pressed into pellet, then pre-sintered at 1200 °C for 3 h. The pre-sintered pellet was further sintered at 1450 °C for 10 h to obtain a dense electrolyte pellet disc with a diameter of 18 mm and thickness of 300  $\mu m$ . To prepare a cathode material slurry, a mixture of LSCoMn and GDC (Gadolinium doped ceria,  $Ce_{0.9}Gd_{0.1}O_2$ , UHSA Anankasei) in a weight ratio of 6:4 was mixed with a binder composed of  $\alpha$ -terpinol and ethyl cellulose. Similarly, an anode material slurry composed of  $La_{0.6}Sr_{0.4}Co_{0.2}Fe_{0.8}O_3$  (LSCF, Fuel cell materials) and GDC was also prepared. The cathode slurry was screen-printed onto the prepared electrolyte-supported pellet, and the anode slurry was coated using the same method on the other side of the electrolyte pellet. The electrode-coated cell was sintered at 1000 °C for 1 h to yield an electrolyte-supported cell, denoted as LSCoMn-GDC/LSGM/LSCF-GDC.

### 2.3. Characterization of materials

The crystal structure, chemical compatibility and phase stability were examined by XRD analysis (Ultima IV, Rigaku), as conducted in the 2 $\theta$  range of 10° to 80° using Cu-K $\alpha$  radiation. SEM (JSM 7401 F, JEOL) and TEM (JEM-2100 F, JEOL) were used to observe the evolution behavior of Co nanoparticles on the surface of the cathode material. The conductivity was measured using a four-probe method under different gas conditions of reducing (20%  $H_2/N_2$ ), oxidizing (air) or electrolysis reaction (30%  $CO/CO_2$ ). The XANES spectra of Co K-edge and Mn K-edge were obtained on the 7D beamline of the Pohang Accelerator Laboratory (PLS-II), in which ATHENA software was used for the XANES analysis. The thermophysical property of LSCoMn was characterized by TGA (SDT Q600, TA instruments) over temperature range from 90 °C to 850 °C at a heating rate of 10 °C/min.  $N_2$  adsorption/desorption analysis at –196 °C was conducted using a Quantachrome apparatus to determine the Brunauer-Emmett-Teller (BET) specific surface area and Barrett-Joyner-Halenda (BJH) pore volume.  $H_2$ -TPR was performed on a flow reactor, where  $H_2$  gas was flowed through the catalyst, and the amount of  $H_2O$  generated by the reduction of the catalyst was measured using GC-MS system (7890B-5977B, Agilent technologies) while raising the temperature from 90 °C to 850 °C at a heating rate of 10 °C/min.  $O_2$ -TPO was also performed over the same reactor where 5%  $O_2/N_2$  mixed gas was flowed through the catalyst, and the amount of  $O_2$  gas was measured using GC-MS system (7890B-5977B, Agilent technologies) while raising the temperature from 90 °C to 850 °C at a heating rate of 10 °C/min. The  $CO_2$ -TPD of the catalyst was also carried out and the gas product was analyzed using GC-MS system (7890B-5977B, Agilent technologies). For  $CO_2$  adsorption on the catalyst,  $CO_2$  was flowed through the catalyst at room temperature for 1 h and purged with He for 3 h. Thereafter, the desorbed  $CO_2$  was analyzed while raising the temperature to 900 °C at a heating rate of 10 °C/min. The Co metal surface area and dispersion of the Co-R.P.LSCoMn were examined with a catalyst analyzer (3flex, Micromeritics) based on CO chemisorption method to calculate turnover frequency (TOF) for the  $CO_2$  electrolysis reaction.

### 2.4. Electrochemical measurement

To test the electrolytic single cell, the fabricated button cell was attached to an alumina tube and sealed with a Pyrex ring sealant. The electrochemical property was measured using the four-probe method with two wires connected to each electrode. Pt mesh and wires were used as the current collector on the anode compartment and Ag wires were used on the cathode side. Details of the apparatus set-up were illustrated on Fig. S1. Prior to the cell tests, temperature was ramped slowly to 850 °C to seal the reaction compartment by melting the Pyrex

ring. Afterward, 20%  $H_2/N_2$  reducing gas at a flow rate of 50 sccm was fed into the cathode compartment for 0.5 h to induce exsolution of Co and to complete reduction of the cathode material, while the anode side was simply exposed to ambient air. Subsequently, a dry gas mixture of 30%  $CO/CO_2$  at a flow rate of 50 sccm was fed into the cathode side for the reaction of  $CO_2$  electrolysis. The electrochemical properties were examined using electrochemical impedance spectroscopy (EIS, MP2, Zive Lab), in which AC impedance was measured in the frequency range from 100 MHz to 10 mHz at the open circuit voltage (OCV) at 850, 800 and 750 °C. A stability test was conducted under a constant current density of 700 mA/cm<sup>2</sup> in the reaction gas mixture of 30%  $CO/CO_2$  at a flow rate of 50 sccm for 12 h operation and the outlet gases were on-line analyzed using a gas chromatography (GC, Agilent 6890) equipped with a thermal conductivity detector (TCD) and a Carboxen 1000 column. The TCD detector was maintained at the temperature of 200 °C and Ar was used as the carrier gas.

### 3. Results

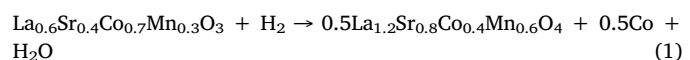
#### 3.1. Characterization of catalysts

XRD analysis was used to investigate structural evolution under the redox reaction condition with particular attention to the appearance of in situ exsolved Co nanoparticles (Fig. 1a). The redox behavior and crystal structure of as-prepared LSCoMn were analyzed after exposure to the reducing atmosphere (20%  $H_2/N_2$ ) at 800 °C for 10 h, followed by the oxidizing condition in the air. No impurity phases other than the pure perovskite phase were detected in the as-prepared LSCoMn

sample. After exposure to the reducing condition, a phase change took place from the perovskite to Ruddlesden-Popper structure, together with an evolution of Co metal nanoparticles as denoted by filled square in the XRD pattern. The presence of Co metal phase definitely explains the exsolution process occurring during the phase transition. This is probably preferential due to the fact that the reduction potential of Co ion is much larger than that of Mn ion [35]. After re-oxidation process, the Ruddlesden-Popper structure appeared to reversibly return to its original perovskite structure; this trend confirms the reversible phase transition under redox conditions. For fabrication of SOEC system, GDC was mixed with the prepared catalyst to increase the ionic conductivity of the cathode electrode, in which the chemical reactivity between catalyst and GDC should be examined as demonstrated in Fig. 1b. The mixture exhibited the XRD peaks of individual perovskite LSCoMn and fluorite GDC without any additional secondary phases or peak shift; this result indicates that the chemical reactivity between the LSCoMn and GDC would be negligible.

To investigate the microstructure evolution of catalyst from reduction process, SEM analysis was performed. No metal nanoparticles were observed on the surface of as-prepared LSCoMn structure (Fig. 2a). However, after exposure to the reducing condition (20%  $H_2/N_2$ ) at 800 °C for 10 h, metal nanoparticles appeared via exsolution process with sizes of about 20–50 nm and they were distributed uniformly on the surface (Fig. 2b). The XRD results (Fig. 1) confirmed that the nanoparticles were of Co metal phase, and the supports were identified as LSCoMn ceramics with Ruddlesden-Popper structure. The morphological characteristics of Co-R.P.LSCoMn were further examined by TEM and EDS (Fig. 2c). The Co nanoparticles of spherical shape appeared to be well attached to the surface of reduced catalyst. To verify compositions of nanoparticles, EDS elemental mapping was conducted; which indicated the existence of La, Sr, Co, Mn and O in the Co-R.P.LSCoMn. Furthermore, only the Co (green) element was uniformly distributed in the exsolved nanoparticles while the other elements were negligible, suggesting that the nanoparticles are composed of pure and dense Co metal.

Local geometric structure and electronic properties of Co and Mn elements in the catalyst were analyzed by XANES recorded at the Co K-edge and Mn K-edge (Fig. 3). For comparison, reference Co compounds such as Co metal,  $CoO$  (99.9%, Sigma Aldrich),  $Co_3O_4$  (99.0%, Alfa Aesar) and  $LaCoO_3$  were plotted together with the samples of LSCoMn, Co-R.P.LSCoMn, and R.P.LSCoMn (Fig. 3a). The Co K-edge XANES graph of LSCoMn (pink line) appears to be similar to that of  $LaCoO_3$  (green line), since both have the same perovskite structure ( $ABO_3$ ) with Co atoms located in the B-sites. Additionally, an analysis of linear combination fitting (LCF) with XANES spectra was performed using ATHENA software in order to estimate the relative composition of Co species in the Co-R.P.LSCoMn (see Fig. S2). It was found that 75.2% Co was in the form of metallic Co and 24.8% Co was present in the Ruddlesden-Popper structure support, which results are very close to the theoretical value (Co metal:Co in R.P. = 72:28) that can be calculated using the phase transition equation as follow.



For the Mn K-edge,  $MnO$  (99.0%, Sigma Aldrich),  $Mn_2O_3$  (99.0%, Sigma Aldrich)  $MnO_2$  (99.9%, Sigma Aldrich),  $LaMnO_3$  and LSCoMn, Co-R.P.LSCoMn were analyzed (Fig. 3b). The Mn K-edge XANES graphs of LSCoMn (pink line) and  $LaMnO_3$  (green line) were similar as they have the same crystal structure of perovskite with Mn located at the B-site. Noticeable differences of the Mn K-edge XANES shape are observed between the LSCoMn and Co-R.P.LSCoMn (blue line), indicating that geometric structures with electronic characteristics of Mn species in the catalyst were significantly changed during the reduction process.

The oxygen vacancies play an important role in SOEC cathode catalyst in regard of  $O^{2-}$  conduction and molecular adsorption. In order to transfer the oxygen ions formed from the cathode reaction to the

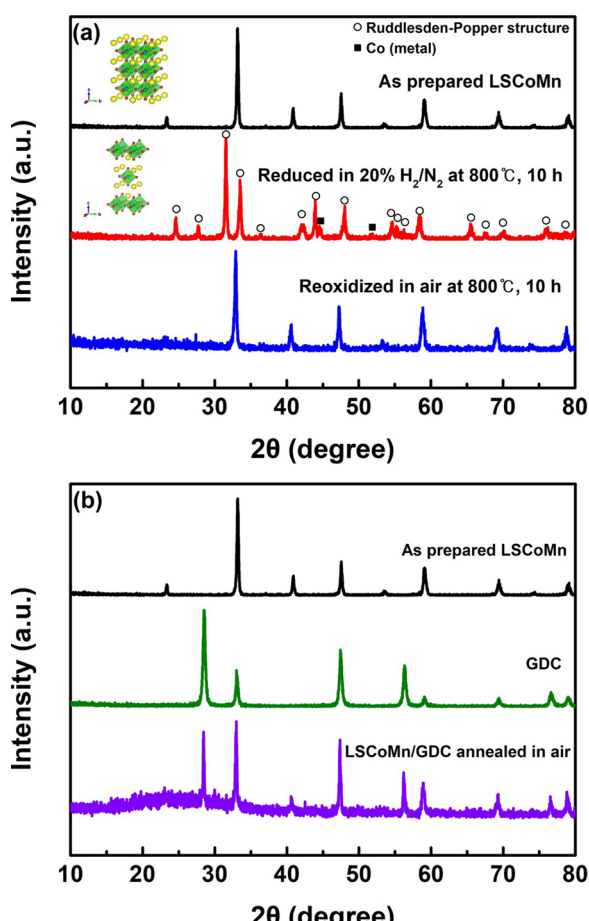
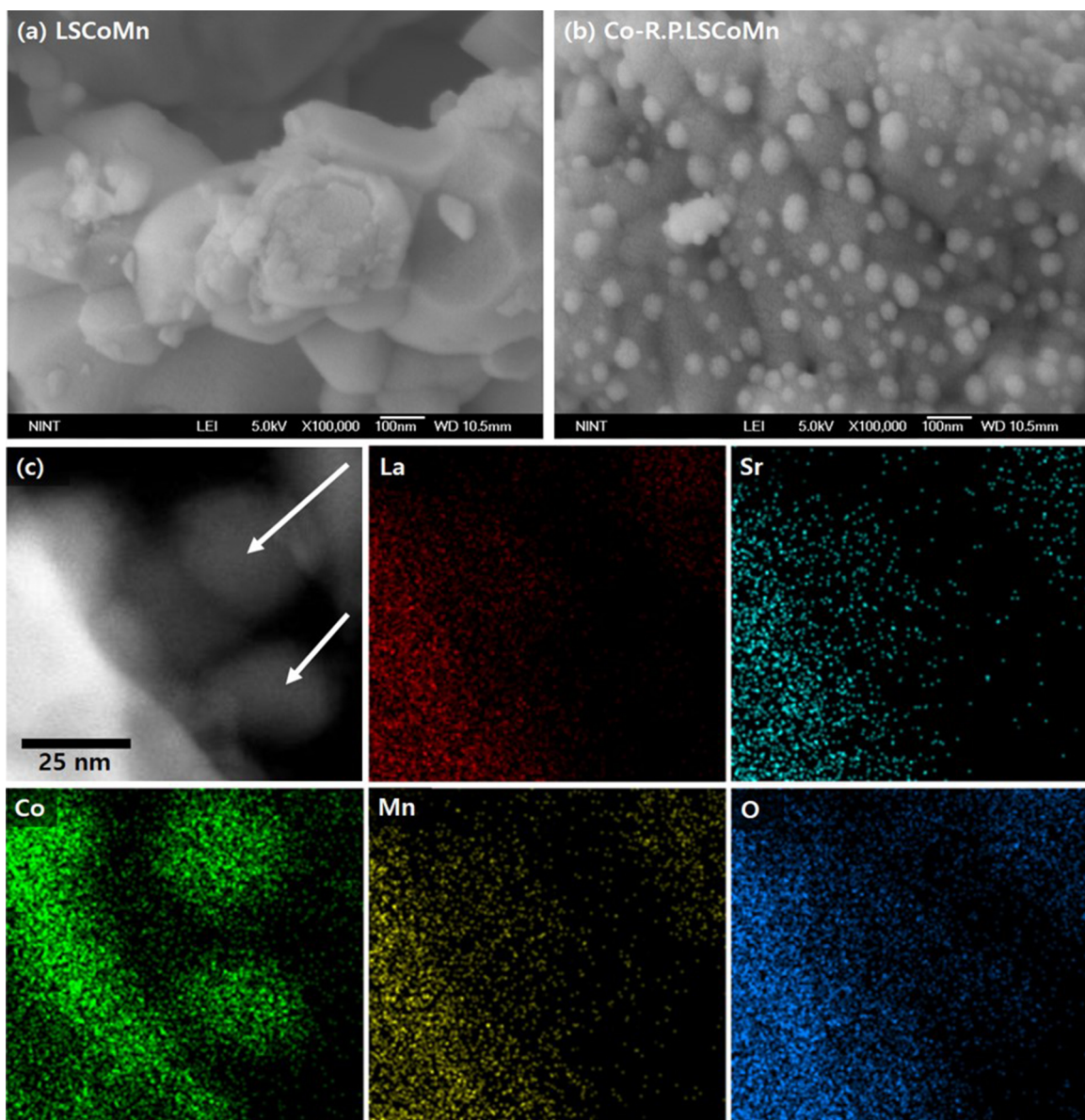


Fig. 1. X-ray diffraction (XRD) patterns of (a) LSCoMn perovskite with redox treatment and (b) LSCoMn mixed with GDC after heat treatment in air at 1000 °C for 1 h.



**Fig. 2.** Scanning electron microscopy (SEM) images of (a) as-calcined LSCoMn and (b) Co-R.P.LSCoMn. (c) Transmission electron microscopy (TEM) and energy-dispersive X-ray spectroscopy (EDS) elemental mappings of (La, Sr, Co, Mn, O) of the Co-R.P.LSCoMn powder.

electrolyte, a decent  $O^{2-}$  conductivity is required. Moreover, the oxygen vacancies formed on the catalyst surface can interact the  $CO_2$  molecules, leading to its adsorption. Consequently, it is necessary to introduce more oxygen vacancies on the catalyst surface. To investigate the information of oxygen vacancy, XANES analysis and TGA measurements were conducted.

The XANES analysis was used to determine the average oxidation state of B-site elements and the information of oxygen vacancies formed in the Co-R.P.LSCoMn. To calculate the average oxidation state of the Co species in the catalyst, a linear relationship between the edge energy position and the known oxidation states of reference samples were investigated (Fig. 3c). The Co-R.P.LSCoMn was found to have two edge energy positions from the first derivative of XANES (Fig. S3a), where the zero oxidation state can be attributed by the metallic Co nanoparticles and the other oxidation number of 2.54 appeared should come from the Co species in the Ruddlesden-Popper support. The oxidation state of the latter Co species in the catalyst seems to be slightly reduced after the phase transition from LSCoMn to Co-R.P.LSCoMn by showing the oxidation number from 2.93 to 2.54. Mn species also showed a decrease in the oxidation number from the same reduction process (3.45→2.92)

(Fig. 3d). On the basis of calculated average oxidation states of Co and Mn, nonstoichiometry ( $\delta$ ) of oxygen can be calculated with an assumption of maintaining electrical neutrality of crystal structure. The  $\delta$  values were estimated to 0.02 for the Co-R.P.LSCoMn ( $La_{1.2}Sr_{0.8}Co_{0.4} Mn_{0.6}O_{3.98}$ ), indicating that the Ruddlesden-Popper support in the form of Co-R.P.LSCoMn possessed the oxygen vacancy contents which could contribute to an increase of the catalytic activity [36].

In order to investigate the phase transition temperature of Co-R.P.LSCoMn and the amount of oxygen vacancies formed around the reaction temperature of  $CO_2$  electrolysis, weight change of the catalyst material with temperature was measured using TGA (Fig. 4a and b). As the temperature increased under the reducing condition, the weight of catalyst decreased, mainly by oxygen loss from the lattice (Fig. 4a). In the temperature ranges of 200 °C to 400 °C, there is a weight loss by liberation of  $H_2O$  (eq. (1)) from the reaction with lattice oxygen while the perovskite structure was still maintained (Fig. S5a). The catalyst weight significantly decreased between 600 °C and 700 °C, indicating that the phase transformation took place to the Ruddlesden-Popper structure with the exsolved Co metal nanoparticles in this range (Fig. S5a). Interestingly, the weight loss of the Co-R.P.LSCoMn was able to be

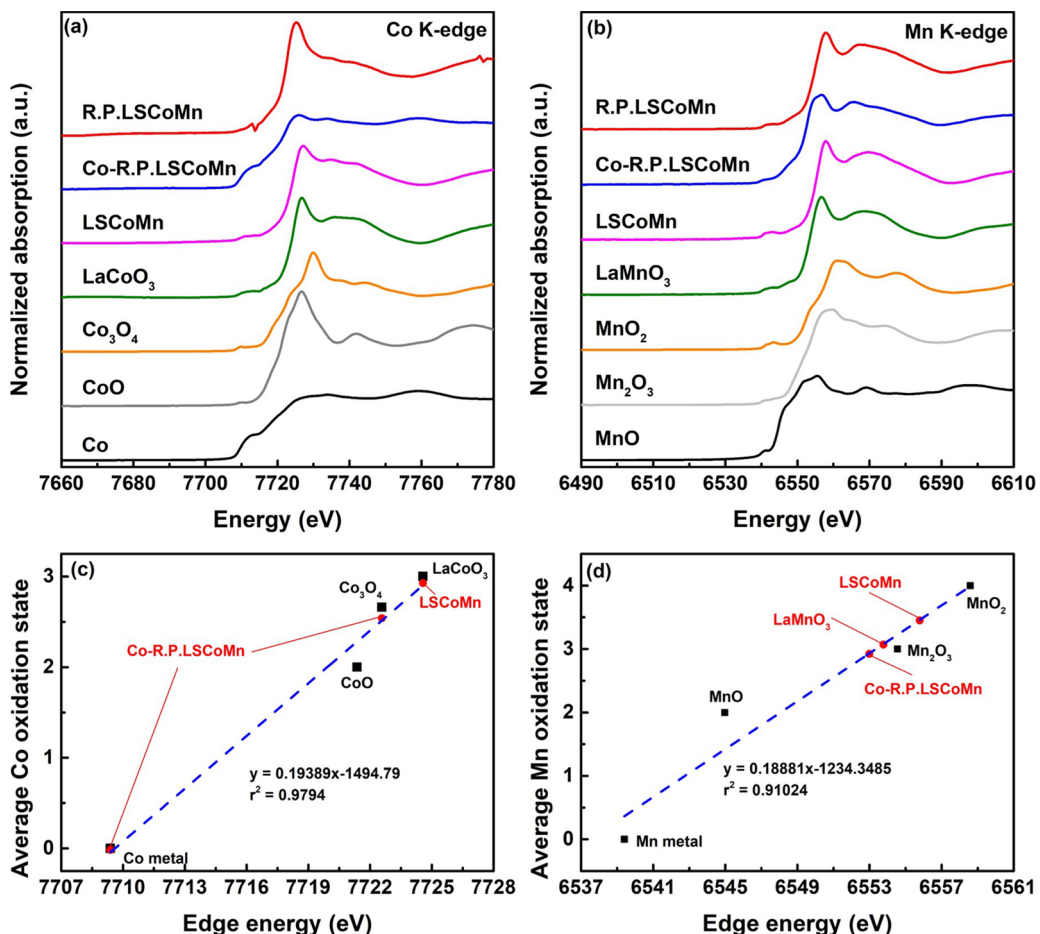
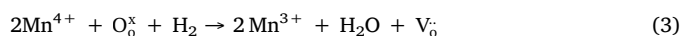
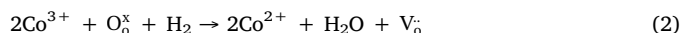


**Fig. 3.** (a) Co K-edge and (b) Mn K-edge XANES spectra of Co and Mn in LSCoMn and Co-R.P.LSCoMn. The average oxidation states of (c) Co and (d) Mn as a function of the edge energy.

recovered almost to its initial one when the temperature was increased in the air (Fig. 4b). This increase of the weight over 300 °C could be attributed to the re-oxidation processes of Co metal to Co<sub>3</sub>O<sub>4</sub> phase (Fig. S5b). The Ruddlesden-Popper structure was maintained until 700 °C then the phase was changed to the perovskite structure after the temperature of 700 °C. The overall weight change of 6.98% was observed by reduction and re-oxidation process of LSCoMn powder. From the assumption that the weight loss is attributed to evolution of oxygen from the lattice, we can calculate  $\delta$  value of 0.20 in the Ruddlesden-Popper support of Co-R.P.LSCoMn; this value is larger than the calculated one from XANES result ( $\delta_{\text{XANES}}$ : 0.02). An additional removal of adsorbed oxygen and lattice oxygen species at high temperatures might be responsible for the larger  $\delta$  from the TGA experiment.

To investigate the reduction and oxidation characteristics of the synthesized catalysts, H<sub>2</sub>-TPR and O<sub>2</sub>-TPO experiments were performed, respectively. Fig. 4c illustrates the H<sub>2</sub>-TPR profile of the synthesized LSCoMn perovskite. The LSCoMn exhibited two regions of peaks at the temperature range of 200–400 °C and 600–700 °C, respectively. In particular, the first region appears to contain two peaks of similar size, which are overlapped. This is due to the fact that the Co and Mn species, the B-site elements of LSCoMn, are reduced as follows.



The Mn<sup>4+</sup> in the structure is first reduced to Mn<sup>3+</sup> [37], and then the Co<sup>3+</sup> is reduced to the Co<sup>2+</sup> [38]. The second region peak is from the reduction of Co<sup>2+</sup> to Co metal during the phase transition of perovskite to Ruddlesden-Popper and Co metal nanoparticles [39].

Furthermore, the positions of these peaks were almost similar to the weight loss position appeared in the TGA, which suggests that the reduction of the B-site elements should lead to the escape of lattice oxygen. Fig. 4d shows the TPO profile of the Co-R.P.LSCoMn, which exhibited two regions with decreasing oxygen amounts at the temperature regions of 250–400 °C and 800–850 °C, respectively. This is in agreement with the weight increase regions in the TGA result (Fig. 4b).

The electrical conductivity of synthesized catalyst was measured with temperature variation under different gas conditions (Fig. 5). In the temperature range of 600–850 °C, the LSCoMn exhibited metallic behavior as its conductivity decreased at the high temperatures. At 850 °C, the LSCoMn showed a high electrical conductivity of 71.3 S/cm under air, whose value might be contributed by coexisted Co<sup>2+</sup>/<sup>3+</sup> pairs in the catalyst. Under the reducing condition (20% H<sub>2</sub>/N<sub>2</sub>), the Co-R.P.LSCoMn exhibited semiconducting behavior like other Ruddlesden-Popper structures [29]. However, its conductivity value of 0.18 S/cm at 850 °C was relatively lower when compared with the normal perovskite materials. In A<sub>x</sub>B<sub>y</sub>O<sub>z</sub> ceramic structure, the A-site element affects the structural properties, and the B-site element contributes to the conductivity and catalytic activity [40]. Ruddlesden-Popper structure (A<sub>2</sub>BO<sub>4</sub>) appears to have a relatively low conductivity because this structure has the fewer B-site elements than the normal perovskite structure (ABO<sub>3</sub>) [27,41]. The electrical conductivity measured under the gas condition of electrolysis reaction (30% CO/CO<sub>2</sub>) was closer to those obtained under the reducing conditions than that obtained in the air, indicating that the catalyst is in the form of Ruddlesden-Popper structure with exsolved Co metal nanoparticles, not as a perovskite, under the electrolysis operation condition.

To calculate turnover frequency (TOF) for CO<sub>2</sub> electrolysis reaction over the catalyst material used here, the amounts of produced CO were

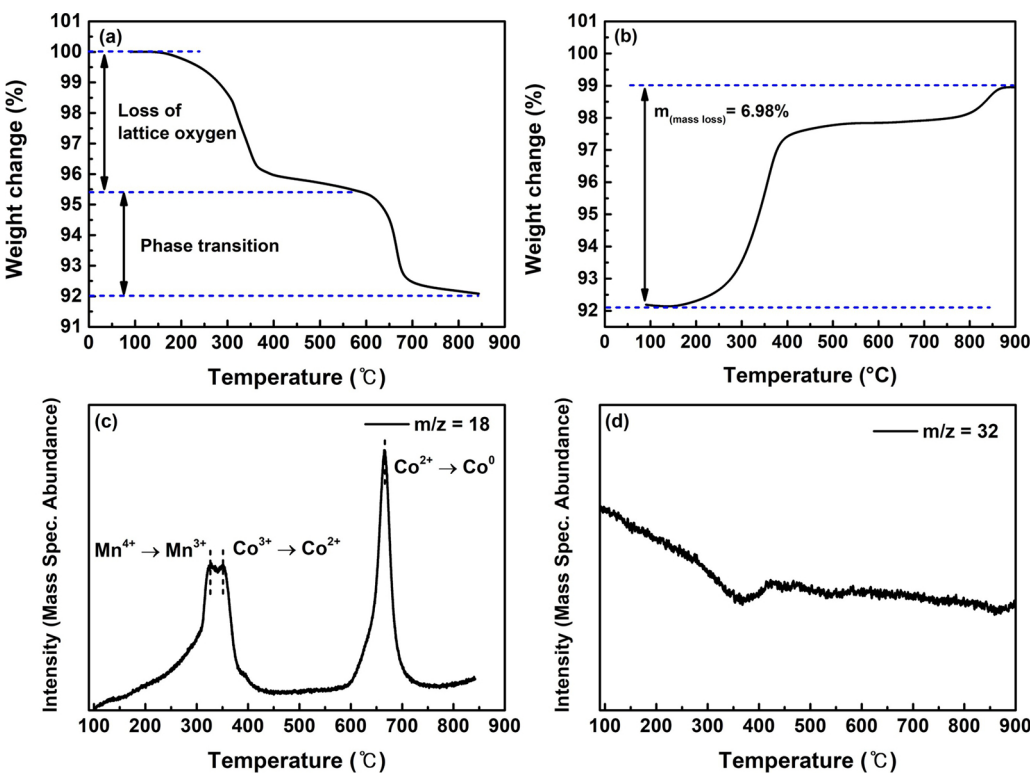


**Fig. 4.** Thermogravimetric analysis (TGA) of (a) LSCoMn in the 20%  $\text{H}_2/\text{N}_2$  condition and (b) Co-R.P.LSCoMn in the air condition at temperature range of 90–850 °C. (c)  $\text{H}_2$ -TPR profile for the LSCoMn and (d)  $\text{O}_2$ -TPO profile for Co-R.P.LSCoMn catalyst at temperature range of 90–850 °C.

employed per areas of the exsolved Co and R.P.LSCoMn support (Supporting information). The exsolved Co metal surface area was obtained from CO chemisorption method and the physical surface area of R.P.LSCoMn was measured by  $\text{N}_2$  gas adsorption/desorption isotherm using the BET method (Table 1, Fig S4). The BET surface area was calculated as ca. 3.66  $\text{m}^2/\text{g}$  and 5.53  $\text{m}^2/\text{g}$  for the Co-R.P.LSCoMn and R.P.LSCoMn, respectively; the Co-R.P.LSCoMn showed a smaller BET surface area than that of R.P.LSCoMn. Also, the BJH pore volume value of Co-R.P.LSCoMn (0.015  $\text{cm}^3/\text{g}$ ) was smaller than that of R.P.LSCoMn (0.024  $\text{cm}^3/\text{g}$ ). This tendency could be attributed by the fact that the Co nanoparticles formed on the surface might obstruct the pores of the R.P.LSCoMn support [42].

To investigate the beneficial effects of the exsolved Co metal nanoparticle on  $\text{CO}_2$  adsorption property,  $\text{CO}_2$ -TPD measurement (Fig. S6) was conducted and compared on the Co-R.P.LSCoMn and R.P.LSCoMn. Both materials showed characteristic  $\text{CO}_2$  desorption peak at temperature region of 700–800 °C, which is typically found in the La-based ceramics [43,44]. The R.P.LSCoMn exhibited an additional peak near 630 °C, which could be attributed to the  $\text{La}_2\text{O}_3$  phase that could be present even in a small amount in R.P.LSCoMn [45] (Fig. S7a). The  $\text{CO}_2$  desorption peak position of the Co-R.P.LSCoMn was located at a relatively higher temperature than that of the R.P.LSCoMn, suggesting that the  $\text{CO}_2$  molecules could be adsorbed stronger to the catalyst surface in presence of the Co nanoparticles on the catalyst surface. Therefore, more  $\text{CO}_2$  molecules are likely to participate in the  $\text{CO}_2$  electrolysis reaction, leading to the enhanced catalytic performance.

### 3.2. Electrocatalytic activity and stability of catalyst

Electrochemical characteristics (I-V curves) of a single cell configuration with Co-R.P.LSCoMn-GDC/LSGM/LSCF-GDC were represented in Fig. 6a at different temperatures. A gas mixture of  $\text{CO}/\text{CO}_2$  with 3:7 vol fraction was supplied to the cathode compartment while the anode was exposed to ambient air. The OCV values were measured to 0.884 V, 0.903 V and 0.931 V at temperatures of 850 °C, 800 °C and

750 °C, respectively; these seem to be slightly lower than the calculated OCVs at the corresponding temperature [27]. The I-V curves represent two regions of the SOEC process at negative currents for the power consumption and of the SOFC process at positive currents for the power generation; in which the shift between the two processes is smooth and continuous, suggesting a high reversibility between the SOEC and SOFC processes [25,26,46]. The current density values measured at 1.3 V were ca. 630  $\text{mA}/\text{cm}^2$  at 850 °C and ca. 430  $\text{mA}/\text{cm}^2$  at 800 °C. When the electrochemical performance is compared with the other catalyst materials that involve a single component exsolution, the Co-R.P.LSCoMn catalyst appears to show the highest current density value at 800 °C and similar reaction condition (Fig. S8, Table S1). In addition, the current density values measured at the thermoneutral voltage, which is about 1.46 V for a dry  $\text{CO}_2$  electrolysis reaction, were ca. 894  $\text{mA}/\text{cm}^2$  at 850 °C and ca. 687  $\text{mA}/\text{cm}^2$  at 800 °C. At this voltage, the applied electrical energy is equivalent to the endothermic energy of the  $\text{CO}_2$  electrolysis reaction for the production of CO and  $\text{O}_2$  without any heat transfer. The current density at 1.3 V decreased with lowering the temperature. The relatively fast reaction kinetics of  $\text{CO}_2$  electrolysis and a small overpotential on the cathode side at high operating temperature might be attributed [46]. Moreover the number of oxygen vacancies on the surface of catalyst could be changed with the operating temperature; these vacancies can readily accommodate and activate non-polar  $\text{CO}_2$  molecules [27,28]. At higher temperatures, the larger amount of surface oxygen vacancies can be formed, leading to increase in the number of  $\text{CO}_2$  molecules that can be accommodated and activated on the surface of catalyst. To further evaluate the electrochemical characteristics, AC impedance spectroscopy was also conducted at different temperatures (Fig. 6b). The Ohmic resistance  $R_\Omega$ , which is value of the intercept of the curve with the x-axis in the high frequency region, is mainly associated with the LSGM electrolyte and the interfacial contact between the electrode and LSGM support [29,47]. The polarization resistance  $R_p$ , which is the difference between the intercepts in the x-axis, could be affected by the interfacial oxygen ion exchange and charge transfer reaction, which are related to  $\text{O}^{2-}$

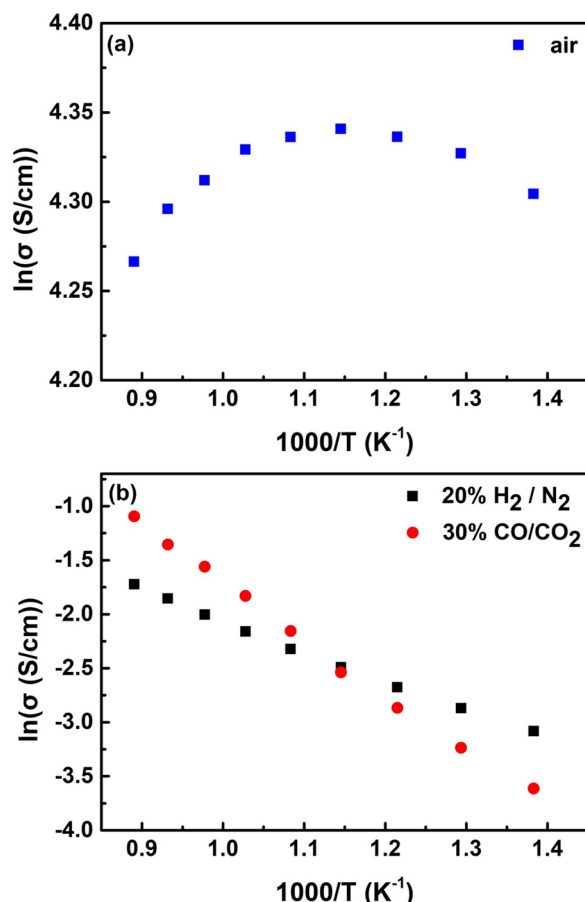


Fig. 5. Electrical conductivity of (a) LSCoMn measured in the air and (b) Co-R.P.LSCoMn measured in 20% H<sub>2</sub>/N<sub>2</sub> and 30% CO/CO<sub>2</sub> at temperature ranges of 450 °C–850 °C.

conductivity and the lengths of triple phase boundary sites (TPBs) [29,47]. Both  $R_{\Omega}$  and  $R_p$  decreased as temperature increased, indicating that the resistance to charge transfer is decreased at higher temperature. As a result, the increased number of reaction sites for CO<sub>2</sub> and the increased charge transfer property may explain the improved electrochemical performance as the temperature increases.

To examine the stability of the cathode during the CO<sub>2</sub> electrolysis reaction, the button cell was operated under a constant applied current density of 700 mA/cm $^2$  in the gas mixture of CO/CO<sub>2</sub> (Fig. 7a). During operation for 12 h, the voltage value was maintained at 1.5 V without any noticeable degradation, confirming that the Co-R.P.LSCoMn cathode material is highly stable under the CO<sub>2</sub> electrolysis condition. Furthermore, the production rates of CO and its Faraday efficiency were calculated with respect to the applied voltage (vs. OCV) (Fig. 7b). The CO production increased as the applied voltage was increased until

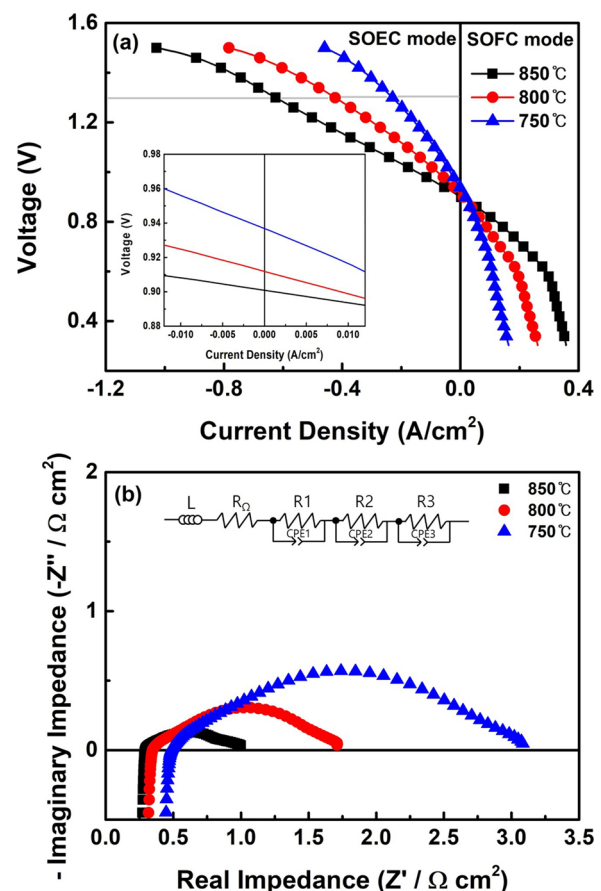


Fig. 6. (a) Current-voltage curves and (b) EIS curves of SOEC with configuration of Co-R.P.LSCoMn-GDC/LSGM/LSCF-GDC for the CO<sub>2</sub> electrolysis.

0.6 V (vs. OCV) at which the production was about 132  $\mu\text{mol min}^{-1} \text{cm}^{-2}$ , but seemed to decrease slightly at 0.8 V. This result could be attributed by the possible damage on the electrode due to the high applied voltage, considering the increase of the  $R_{\Omega}$  and  $R_p$  values after high voltage operation test (Fig. S9). The Faraday efficiency of Co-R.P.LSCoMn cell showed a maximum value of ca. 97% or larger in Table S1. These high current density and Faraday efficiency of Co-R.P.LSCoMn developed in this study could give an opportunity to serve as the promising catalyst for the CO<sub>2</sub> electrolysis reaction.

To confirm the effect of Co metal nanoparticles for the CO<sub>2</sub> electrolysis process, a button type single cell was fashioned of R.P.LSCoMn as the cathode under the same experimental condition and its electrochemical characteristics were analyzed (Fig. S7b and Fig. S7c). When using the R.P.LSCoMn cathode, measured current density was 170 mA/cm $^2$  at 1.3 V and 850 °C (Fig. S7b); this value is smaller than the cell with the Co-R.P.LSCoMn cathode, indicating that the Co metal

Table 1  
Physicochemical properties and electrocatalytic activities of the catalysts for CO<sub>2</sub> electrolysis.

Catalysts	BET surface area (m $^2$ g $^{-1}$ )	BJH pore volume (cm $^3$ g $^{-1}$ )	Current Density (mA·cm $^{-2}$ at 1.3 V)	Production rate of CO <sup>a</sup> (μmol·min $^{-1}$ ·cm $^{-2}$ elec)	Production rate of CO <sup>b</sup> (μmol·min $^{-1}$ ·cm $^{-2}$ catalyst)	TOF <sub>Co</sub> <sup>c</sup> (sec $^{-1}$ )
R.P.LSCoMn	5.53	0.024	170	42.8	0.124	–
Co-R.P.LSCoMn	3.66	0.015	630	132.3	0.609	9.36 <sup>d</sup> 8.99 <sup>e</sup>

<sup>a</sup> Production rate of CO per minute per unit area of electrode at an applied voltage of 0.6 V (vs OCV).

<sup>b</sup> Production rate of CO per minute per unit area of catalyst at an applied voltage of 0.6 V (vs OCV).

<sup>c</sup> The turnover frequency (TOF) value for CO production at a potential of 0.6 V (vs OCV), which is defined as the rate of CO molecules produced per surface Co atom.

<sup>d</sup> The calculated TOF value based on the electrical current measured.

<sup>e</sup> The calculated TOF value based on the production rate of CO quantified by GC.

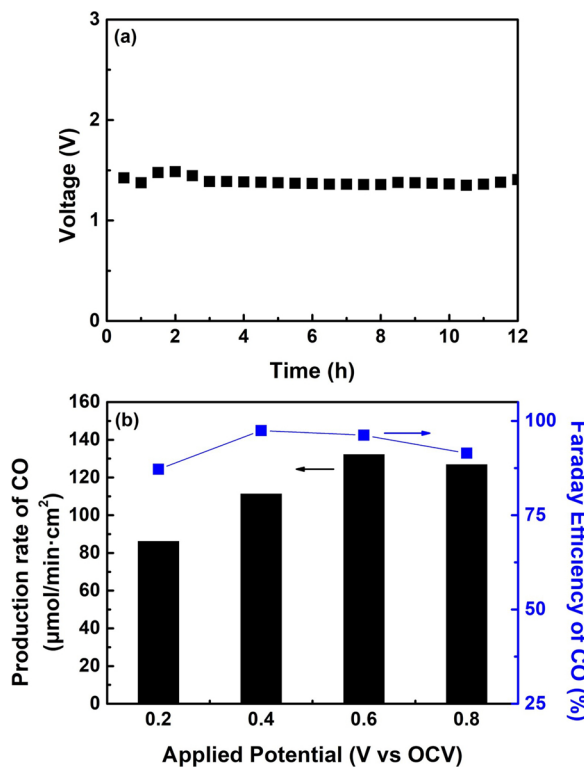


**Fig. 7.** (a) Voltage profile of the cell with Co-R.P.LSCoMn cathode at the constant current density of 700 mA/cm<sup>2</sup> at 850 °C. (b) Production rate of CO of the cell with Co-R.P.LSCoMn cathode at different applied potentials and the corresponding Faraday efficiency.

nanoparticles could substantially improve the catalytic activity in the CO<sub>2</sub> electrolysis reaction. In addition, the EIS result showed that the R<sub>p</sub> value of the cell with R.P.LSCoMn cathode was larger than that of Co-R.P.LSCoMn (Fig. S7c), indicating that the exsolved Co metal nanoparticles could contribute to the facilitated charge transfer process for CO<sub>2</sub> electrolysis. The production rates of CO per surface area of R.P.LSCoMn and Co-R.P.LSCoMn used as SOEC cathode catalysts for CO<sub>2</sub> electrolysis are displayed and summarized in Fig. S7d and Table 1, respectively. The R.P.LSCoMn cell showed the relatively lower activity than the Co-R.P.LSCoMn cell in terms of CO production rate and Faraday efficiency which are based on the outlet gas composition analysis. The SOEC with Co-R.P.LSCoMn cathode exhibited the substantially higher production rate of CO (0.609 μmol min<sup>-1</sup> cm<sup>-2</sup><sub>catalyst</sub>) compared to the case without Co nanoparticles (0.124 μmol min<sup>-1</sup> cm<sup>-2</sup><sub>catalyst</sub>). The turnover frequency (TOF) values for CO production at a potential of 0.6 V (vs OCV), which is defined as the rate of CO molecules produced per surface Co atom, were calculated based on two different ways: 1) one is based on the current density value [48,49] and 2) the other is based on the production rate of CO that can be quantified by GC (for detailed calculation, see Supporting information). The calculated TOF values were 9.36 s<sup>-1</sup> for using the current density and 8.99 s<sup>-1</sup> for using the production rate, suggesting that these two methods are quite consistent. The slight difference is thought to be from the loss of Faraday efficiency to convert CO<sub>2</sub> to CO. Also, these values comparable with the TOF values for the typical catalytic reactions [42,50–53]. For example, in a CO<sub>2</sub> reforming reaction with CH<sub>4</sub> using metal nanoparticles on a ceramic support as a catalyst, the TOF has values of 1.0 to 4.9 s<sup>-1</sup> [51].

The electrochemical performance of a single cell made of Co impregnated R.P.LSCoMn cathode was investigated to compare the differences with respect to the formation method of Co metal nanoparticles. The cell with the Co impregnated R.P.LSCoMn cathode exhibits higher electrochemical performance than that of R.P.LSCoMn

cathode (Fig. S7b), but is shown much lower performance than that of the Co exsolved Co-R.P.LSCoMn catalyst material. The EIS results revealed the similar conclusion to those of I-V curves (Fig. S7c). In addition, during the stability test, the Co impregnated R.P.LSCoMn cell exhibited that the voltage was fluctuated very unstably than that of Co-R.P.LSCoMn cell (Fig. S7e). In Fig. S7f for the EIS results, the R<sub>p</sub> value of the cell with Co-R.P.LSCoMn cathode was increased slightly after the 12 h operation, which can be ascribed by the decrease in the TPBs from agglomeration of the exsolved Co metal nanoparticles [54]. However, the Co impregnated R.P.LSCoMn cell showed a much larger R<sub>p</sub> value increase than that of Co-R.P.LSCoMn, suggesting that the impregnated Co would be much more vulnerable to the agglomeration of Co nanoparticle. To support this, microstructures of the electrode before and after the stability test were examined by SEM analysis (Fig. S10). The exsolved Co metal nanoparticles of Co-R.P.LSCoMn cathode showed slightly increased particle size (Fig. S10a and S10b), however, the impregnated Co nanoparticles appeared to experience much bigger size difference before and after the stability test (Fig. S10c and S10d). These slight increases in the size of Co nanoparticles and the R<sub>p</sub> value could take place during the activation of the electrode in the early stage of the test, however, the size of the nanoparticles and the R<sub>p</sub> value appears to be maintained after the initial period [55].

#### 4. Discussion

The catalysts with in situ exsolved metallic Co nanoparticles on Ruddlesden-Popper material (i.e., Co-R.P.LSCoMn) were successfully synthesized and used as the SOEC cathode catalyst to convert CO<sub>2</sub> into CO at a high reaction rate. The single cell fabricated with the Co-R.P.LSCoMn exhibited outstanding electrochemical performance and stability with a very high Faraday efficiency up to 97%. The rationale for such high catalytic and electrochemical performance of the proposed material can be explained and understood by several factors as discussed below.

The high oxygen vacancy concentration of the R.P.LSCoMn support could contribute to the highly improved electrolysis performance of Co-R.P.LSCoMn catalyst. In the ceramic electrodes, the oxygen vacancies can serve as charge carriers for oxygen ions. Therefore, with the higher oxygen vacancy concentration, the higher O<sup>2-</sup> conductivity value of the electrode can be expected, resulting in an increase of the catalytic activity. In addition, the oxygen vacancy formed on the catalyst surface should act as the adsorption sites for CO<sub>2</sub> molecules, therefore the high concentration of oxygen vacancies is likely to allow more CO<sub>2</sub> molecules to participate in the electrolysis reaction. The TGA results suggested that the Co-R.P.LSCoMn catalyst synthesized in this study contains a high oxygen vacancy concentration ( $\delta_{TGA}$ : 0.20). Consequently, the high concentration of oxygen vacancy formed on the Co-R.P.LSCoMn should contribute to the enhanced O<sup>2-</sup> conductivity and the enlarged adsorption sites for the CO<sub>2</sub>, both leading to the improved catalytic performance of the CO<sub>2</sub> electrolysis reaction in this work.

The relatively low temperature used for the preparation of our catalyst, as compared with the typical ceramic catalyst materials for the SOEC, should be of another reason for the high activity. The Ruddlesden-Popper structured ceramics are used as an electrode due to their beneficial properties such as good O<sup>2-</sup> conductivity and fast surface oxygen exchange reaction. However, high calcination temperature up to 1350 °C is typically required for the direct synthesis of the Ruddlesden-Popper structure, which can increase the particle size along with reduction of TPBs. The Co-R.P.LSCoMn synthesized in this study is of a typical Ruddlesden-Popper structure, however, this can be synthesized even at relatively low temperature by reducing perovskite (LSCoMn) at 800 °C. Therefore, the smaller particles with the relatively larger TPBs can be obtained in this Co-R.P.LSCoMn catalyst than the typical preparation methods of Ruddlesden-Popper structure.

Moreover, the Co-R.P.LSCoMn catalyst reveals very stable structured properties, which is highly desirable for the high temperature

SOFC or SOEC system. Some La-based materials such as LSCF are subjected to form insulating phases of  $\text{La}_2\text{O}_3$  or  $\text{SrO}$  in the operating condition, in which these phases should give a deleterious effect on the electrical conduction, leading to a degraded catalytic performance. However, the Co-R.P.LSCoMn exhibits good phase stability without forming any insulating phases such as  $\text{La}_2\text{O}_3$ , only producing the active phases of Ruddlesden-Popper structure and the exsolved Co metal nanoparticles as shown in Fig. 1a. With the high phase stability, the formation of oxygen vacancies ( $\text{V}_\text{o}$ ) is also promoted according to the eq. (2) and (3) [29]; the B-site elements of Co-R.P.LSCoMn can be more reduced without separation of the A-site elements.

As far as the metal nanoparticles are concerned, the exsolved Co metal nanoparticles on the Ruddlesden-Popper materials can significantly improve the electrochemical performance and stability of  $\text{CO}_2$  electrolysis reaction. As shown in Fig. S7b, the exsolved metallic Co nanoparticles can improve electrochemical performance significantly, as compared to those that the Co nanoparticles are not present. One of the roles of the metallic Co nanoparticles is to enhance the adsorption capacity of  $\text{CO}_2$  molecules. The  $\text{CO}_2$ -TPD results confirmed that the Co metal nanoparticles on the ceramic support are able to more strongly adsorb the  $\text{CO}_2$  molecules on the catalyst surface (Fig. S6), in which the more  $\text{CO}_2$  molecules could remain bonded to the catalyst even at high temperatures compared to the cases without metal nanoparticles. Thus, as the adsorption capacity of the catalyst for the  $\text{CO}_2$  molecule is increased, the more  $\text{CO}_2$  molecules are possibly involved in the reaction, resulting in the better electrolysis performance. The other role of the exsolved Co nanoparticles is contribution to the stability of the SOEC single cell during the  $\text{CO}_2$  electrolysis due to the tolerance against agglomeration and coking. Generally, the exsolved metal nanoparticles are strongly adhered to a support with less coalescence and agglomeration than the cases of externally deposited nanoparticles using the typical impregnation method [54]. In addition, the performance degradation due to the carbon deposition that may also occur in the  $\text{CO}_2$  electrolysis process could be alleviated for the cases with the exsolved nanoparticles [54], which was also observed in this work with negligible cell degradation. The stability test of cell with Co impregnated R.P.LSCoMn cathode showed that due to the relatively weak interaction between impregnated nanoparticles and the R.P.LSCoMn support compared to exsolved case, coalescence and agglomeration of the small metal nanoparticles easily occurred much faster (Fig. S10), resulting in unstable performance during a 12 h operation test (Fig. S7e). Also, the result of the relatively high  $R_p$  value of Co impregnated R.P.LSCoMn cell may be speculated by decreased in lengths of TPBs caused by agglomeration and carbon deposition (Fig. S7f). As a result, the exsolved Co metal nanoparticles on the ceramic support increased the adsorption capacity for  $\text{CO}_2$  molecules and the production rate of CO with a high degree of stability over the SOEC single cell.

## 5. Conclusions

We synthesized a promising cathode catalyst material for SOEC systems and evaluated its catalytic activity for  $\text{CO}_2$  reduction to CO. This catalyst material contained Co metal nanoparticles, which were reversibly and in situ formed during the structural transition on the surface of a Ruddlesden-Popper structured ceramic backbone. The catalyst was fabricated by reducing LSCoMn structure in 20%  $\text{H}_2/\text{N}_2$  at 800 °C, and Co nanoparticles and Ruddlesden-Popper phase were obtained without forming any other impurities at a relatively mild temperature. Over the single cell with Co-R.P.LSCoMn cathode, a high current density of 630 mA/cm<sup>2</sup> was accomplished at a voltage of 1.3 V and temperature of 850 °C, together with a Faraday efficiency of 95% or greater. More interestingly, the single cell with the cathode developed in this study exhibited an excellent stability with no sign of degradation as observed by galvanostatic tests under the  $\text{CO}_2$  electrolysis condition. The presence of uniformly distributed Co metal nanoparticles and high

oxygen vacancy contents could contribute greatly to the catalytic activity for the  $\text{CO}_2$  electrolysis. This Ruddlesden-Popper structured catalyst with in situ exsolved Co metal nanoparticles is consequently a promising cathode material for  $\text{CO}_2$  electrolysis.

## Acknowledgments

This research was supported by Basic Science Research Program through the National Research Foundation of Korea (NRF) funded by the Ministry of Science and ICT (NRF-2017R1A2B2012318), and also by the Korea Institute of Energy Technology Evaluation and Planning (KETEP) and the Ministry of Trade, Industry & Energy (MOTIE) of the Republic of Korea (20172010106300).

## Appendix A. Supplementary data

Supplementary material related to this article can be found, in the online version, at doi:<https://doi.org/10.1016/j.apcatb.2019.02.013>.

## References

- [1] Y. Wang, T. Liu, L. Lei, F. Chen, High temperature solid oxide  $\text{H}_2\text{O}/\text{CO}_2$  co-electrolysis for syngas production, *Fuel Process. Technol.* 161 (2017) 248–258, <https://doi.org/10.1016/j.fuproc.2016.08.009>.
- [2] G. Tsekouras, J.T.S. Irvine, The role of defect chemistry in strontium titanates utilized for high temperature steam electrolysis, *J. Mater. Chem.* 21 (2011) 9367–9376, <https://doi.org/10.1039/C1JM11313E>.
- [3] Y. Zheng, J. Wang, B. Yu, W. Zhang, J. Chen, J. Qiao, J. Zhang, A review of high temperature co-electrolysis of  $\text{H}_2\text{O}$  and  $\text{CO}_2$  to produce sustainable fuels using solid oxide electrolysis cells (SOECs): advanced materials and technology, *Chem. Soc. Rev.* 46 (2017) 1427–1463, <https://doi.org/10.1039/C6CS00403B>.
- [4] L. Zhang, S. Hu, X. Zhu, W. Yang, Electrochemical reduction of  $\text{CO}_2$  in solid oxide electrolysis cells, *J. Energy Chem.* 26 (2017) 593–601, <https://doi.org/10.1016/j.jechem.2017.04.004>.
- [5] S. Kim, M. Park, H. Kim, K.J. Yoon, J. Son, J. Lee, B. Kim, J. Lee, J. Hong, In-situ nano-alloying Pd-Ni for economical control of syngas production from high-temperature thermos-electrochemical reduction of steam/ $\text{CO}_2$ , *Appl. Catal. B: Environ.* 200 (2017) 265–273, <https://doi.org/10.1016/j.apcatb.2016.07.008>.
- [6] S. Wang, H. Tsuruta, M. Asanuma, T. Ishihara, Ni–Fe–La(Sr)Fe(Mn)O<sub>3</sub> as a new active cermet cathode for intermediate-temperature  $\text{CO}_2$  electrolysis using a LaGaO<sub>3</sub>-based electrolyte, *Adv. Energy Mater.* 5 (2015) 1401003, , <https://doi.org/10.1002/aenm.201401003>.
- [7] X. Yue, J.T.S. Irvine, Alternative cathode material for  $\text{CO}_2$  reduction by high temperature solid oxide electrolysis cells, *J. Electrochem. Soc.* 159 (2012) F442–F448, <https://doi.org/10.1149/2.040208jes>.
- [8] E.P. Murray, T. Tsai, S.A. Barnett, A direct-methane fuel cell with a ceria-based anode, *Nature* 400 (1999) 649–651, <https://doi.org/10.1038/23220>.
- [9] W. Qi, Y. Gan, D. Yin, Z. Li, G. Wu, K. Xie, Y. Wu, Remarkable chemical adsorption of manganese-doped titanate for direct carbon dioxide electrolysis, *J. Mater. Chem. A* 2 (2014) 6904–6915, <https://doi.org/10.1039/c4ta00344f>.
- [10] A. Hauch, S.D. Ebbesen, S.H. Jensen, M. Mogensen, Highly efficient high temperature electrolysis, *J. Mater. Chem.* 18 (2008) 2331–2340, <https://doi.org/10.1039/b718822f>.
- [11] E.C. Shin, P.A. Ahn, H.H. Seo, J.M. Jo, S.D. Kim, S.K. Woo, J.H. Yu, J. Mizusaki, J.S. Lee, Polarization mechanism of high temperature electrolysis in a Ni–YSZ/YSZ/LSM solid oxide cell by parametric impedance analysis, *Solid State Ion.* 232 (2013) 80–96, <https://doi.org/10.1016/j.ssi.2012.10.028>.
- [12] M.H. Pihlatie, A. Kaiser, M.J. Mogensen, Redox stability of SOFC: thermal analysis of Ni–YSZ composites, *Solid State Ion.* 180 (2009) 1100–1112, <https://doi.org/10.1016/j.ssi.2009.04.011>.
- [13] M.H. Pihlatie, H.L. Frandsen, A. Kaiser, M.J. Mogensen, Continuum mechanics simulations of NiO–Ni–YSZ composites during reduction and re-oxidation, *J. Power Sources* 195 (2010) 2677–2690, <https://doi.org/10.1016/j.jpowsour.2009.11.079>.
- [14] E. Ioannidou, C. Neofytidis, L. Sygellou, D.K. Niakolas, Au-doped Ni/GDC as an improved cathode electrocatalyst for  $\text{H}_2\text{O}$  electrolysis in SOECs, *Appl. Catal. B: Environ.* 236 (2018) 253–264, <https://doi.org/10.1016/j.apcatb.2018.05.017>.
- [15] K. Zhao, X. Hou, Q. Bkour, M. Grant Norton, S. Ha, NiMo–ceria–zirconia catalytic reforming layer for solid oxide fuel cells running on a gasoline surrogate, *Appl. Catal. B: Environ.* 224 (2018) 500–507, <https://doi.org/10.1016/j.apcatb.2017.10.067>.
- [16] Y. Li, Y. Gan, Y. Wang, K. Xie, Y. Wu, Composite cathode based on Ni-loaded  $\text{La}_{0.75}\text{Sr}_{0.25}\text{Cr}_{0.5}\text{Mn}_{0.5}\text{O}_{3-\delta}$  for direct steam electrolysis in an oxide-ion-conducting solid oxide electrolyzer, *Int. J. Hydrog. Energy* 38 (2013) 10196–10207, <https://doi.org/10.1016/j.ijhydene.2013.06.057>.
- [17] R. Xing, Y. Wang, Y. Zhu, S. Liu, C. Jin, Co-electrolysis of steam and  $\text{CO}_2$  in a solid oxide electrolysis cell with  $\text{La}_{0.75}\text{Sr}_{0.25}\text{Cr}_{0.5}\text{Mn}_{0.5}\text{O}_{3-\delta}$ –Cu ceramic composite electrode, *J. Power Sources* 274 (2015) 260–264, <https://doi.org/10.1016/j.jpowsour.2014.10.066>.
- [18] A. Jun, J. Kim, J. Shin, G. Kim, Achieving high efficiency and eliminating

degradation in solid oxide electrochemical cells using high oxygen-capacity perovskite, *Angew. Chem. Int. Ed.* 55 (2016) 12512–12515, <https://doi.org/10.1002/anie.201606972>.

[19] X. Zhang, L. Ye, J. Hu, W. Jiang, C.J. Tseng, K. Xie, Perovskite LSCM impregnated with vanadium pentoxide for high temperature carbon dioxide electrolysis, *Electrochim. Acta* 212 (2016) 32–40, <https://doi.org/10.1016/j.electacta.2016.06.137>.

[20] Y. Gan, Q. Qin, S. Chen, Y. Wang, D. Dong, K. Xie, Y. Wu, Composite cathode  $\text{La}_{0.4}\text{Sr}_{0.4}\text{TiO}_{3-\delta}-\text{Ce}_{0.8}\text{Sm}_{0.2}\text{O}_{2-\delta}$  impregnated with Ni for high-temperature steam electrolysis, *J. Power Sources* 245 (2014) 245–255, <https://doi.org/10.1016/j.jpowsour.2013.06.107>.

[21] Y. Li, Y. Wang, W. Doherty, K. Kie, Y. Wu, Perovskite chromates cathode with ex-solved iron nanoparticles for direct high-temperature steam electrolysis, *ACS Appl. Mater. Interfaces* 5 (2013) 8553–8562, <https://doi.org/10.1021/am402013z>.

[22] S. Wu, D. Dong, Y. Wang, W. Doherty, K. Xie, Y. Wu, Perovskite chromates cathode with resolved and anchored nickel nano-particles for direct high-temperature steam electrolysis, *J. Power Sources* 246 (2014) 346–355, <https://doi.org/10.1016/j.jpowsour.2013.07.082>.

[23] Y. Li, K. Xie, S. Chen, H. Li, Y. Zhang, Y. Wu, Efficient carbon dioxide electrolysis based on perovskite cathode enhanced with nickel nanocatalyst, *Electrochim. Acta* 153 (2015) 325–333, <https://doi.org/10.1016/j.electacta.2014.11.151>.

[24] W. Qi, C. Ruan, G. Wu, Y. Zhang, Y. Wang, K. Xie, Y. Wu, Reversibly in-situ anchoring copper nanocatalyst in perovskite titanate cathode for direct high-temperature steam electrolysis, *Int. J. Hydrog. Energy* 39 (2014) 5485–5496, <https://doi.org/10.1016/j.ijhydene.2014.01.108>.

[25] S. Liu, Q. Liu, X. Fu, J.L. Luo, Cogeneration of ethylene and energy in protonic fuel cell with an efficient and stable anode anchored with in-situ exsolved functional metal nanoparticles, *Appl. Catal. B: Environ.* 220 (2018) 283–289, <https://doi.org/10.1016/j.apcatb.2017.08.051>.

[26] D. Zubenko, S. Singh, B.A. Rosen, Exsolution of Re-alloy catalysts with enhanced stability for methane dry reforming, *Appl. Catal. B: Environ.* 209 (2017) 711–719, <https://doi.org/10.1016/j.apcatb.2017.03.047>.

[27] S. Liu, Q. Liu, J.L. Luo, Highly stable and efficient catalyst with in situ exsolved Fe–Ni alloy nanospheres socketed on an oxygen deficient perovskite for direct  $\text{CO}_2$  electrolysis, *ACS Catal.* 6 (2016) 6219–6228, <https://doi.org/10.1021/acscatal.6b01555>.

[28] S. Liu, Q. Liu, J.L. Luo,  $\text{CO}_2$ -to-CO conversion on layered perovskite with in situ exsolved Co–Fe alloy nanoparticles: an active and stable cathode for solid oxide electrolysis cells, *J. Mater. Chem. A* 4 (2016) 17521–17528, <https://doi.org/10.1039/c6ta06365a>.

[29] Y.S. Chung, T. Kim, T.H. Shin, H. Yoon, S. Park, N.M. Sammes, W.B. Kim, J.S. Chung, In situ preparation of a  $\text{La}_{1.2}\text{Sr}_{0.8}\text{Mn}_{0.4}\text{Fe}_{0.6}\text{O}_4$  Ruddlesden–Popper phase with exsolved Fe nanoparticles as an anode for SOFCs, *J. Mater. Chem. A* 5 (2017) 6437–6446, <https://doi.org/10.1039/c6ta09692a>.

[30] X. Huang, T.H. Shin, J. Zhou, J.T.S. Irvine, Hierarchically nanoporous  $\text{La}_{1.7}\text{Ca}_{0.3}\text{CuO}_{4-\delta}$  and  $\text{La}_{1.7}\text{Ca}_{0.3}\text{Ni}_x\text{Cu}_{1-x}\text{O}_{4-\delta}$  ( $0.25 \leq x \leq 0.75$ ) as potential cathode materials for IT-SOFCs, *J. Mater. Chem. A* 3 (2015) 13468–13475, <https://doi.org/10.1039/c5ta00983a>.

[31] Y. Chen, B. Qian, G. Yang, D. Chen, Z. Shao, Insight into an unusual lanthanum effect on the oxygen reduction reaction activity of Ruddlesden–Popper-type cation–nonstoichiometric  $\text{La}_{2-x}\text{NiO}_{4+\delta}$  ( $x = 0–0.1$ ) oxides, *J. Mater. Chem. A* 3 (2015) 6501–6508, <https://doi.org/10.1039/c4ta07176>.

[32] J. Zhou, G. Chen, K. Wu, Y. Cheng, The performance of  $\text{La}_{0.6}\text{Sr}_{1.4}\text{MnO}_4$  layered perovskite electrode material for intermediate temperature symmetrical solid oxide fuel cells, *J. Power Sources* 270 (2014) 418–425, <https://doi.org/10.1016/j.jpowsour.2014.06.163>.

[33] Y. Ling, F. Wang, Y. Okamoto, T. Nakamura, K. Amezawa, Oxygen non-stoichiometry and thermodynamic quantities in the Ruddlesden–Popper oxides  $\text{La}_x\text{Sr}_3 - x\text{Fe}_2\text{O}_7 - \delta$ , *Solid State Ion.* 288 (2016) 298–302, <https://doi.org/10.1016/j.jssi.2016.01.016>.

[34] E.S. Raj, K.F.E. Pratt, S.J. Skinner, I.P. Parkin, J.A. Kilner, High conductivity  $\text{La}_{2-x}\text{Sr}_x\text{Cu}_{1-y}(\text{Mg}, \text{Al})\text{O}_4$  solid state metal oxide gas sensors with the  $\text{K}_2\text{NiF}_4$  structure, *Chem. Mater.* 18 (2006) 3351–3355, <https://doi.org/10.1021/cm060520e>.

[35] E.R. Stobbe, B.A. de Boer, J.W. Geus, The reduction and oxidation behaviour of manganese oxides, *Catal. Today* 47 (1999) 161–167, [https://doi.org/10.1016/S0920-5861\(98\)00296-X](https://doi.org/10.1016/S0920-5861(98)00296-X).

[36] D. Lee, H.N. Lee, Controlling oxygen mobility in Ruddlesden–Popper oxides, *Materials* 10 (2017) 368, <https://doi.org/10.3390/ma10040368>.

[37] J. Zhang, Y. Li, L. Wang, C. Zhang, H. He, Catalytic oxidation of formaldehyde over manganese oxides with different crystal structures, *Catal. Sci. Technol.* 5 (2015) 2305–2313, <https://doi.org/10.1039/c4cy01461h>.

[38] G. Zou, Y. Xu, S. Wang, M. Chen, W. Shangguan, The synergistic effect in Co–Ce oxides for catalytic oxidation of diesel soot, *Catal. Sci. Technol.* 5 (2015) 1084–1092, <https://doi.org/10.1039/c4cy01141d>.

[39] K. Sutthiumporn, T. Maneerung, Y. Kathiraser, S. Kawi,  $\text{CO}_2$  dry-reforming of methane over  $\text{La}_{0.8}\text{Sr}_{0.2}\text{Ni}_{0.8}\text{Mn}_{0.2}\text{O}_3$  perovskite ( $\text{M} = \text{Bi}, \text{Co}, \text{Cr}, \text{Cu}, \text{Fe}$ ): roles of lattice oxygen on C–H activation and carbon suppression, *Int. J. Hydrog. Energy* 37 (2012) 11195–11207, <https://doi.org/10.1016/j.ijhydene.2012.04.059>.

[40] S. Liu, K.T. Chuang, J.L. Liu, Double-layered perovskite anode with in situ exsolution of a Co–Fe alloy to cogenerate ethylene and electricity in a proton-conducting ethane fuel cell, *ACS Catal.* 6 (2016) 760–768, <https://doi.org/10.1021/acscatal.5b02296>.

[41] Q. Liu, X. Dong, G. Xia, F. Zhao, F. Chen, A novel electrode material for symmetrical SOFCs, *Adv. Mater.* 22 (2010) 5478–5482, <https://doi.org/10.1002/adma.201001044>.

[42] S. Sengupta, K. Ray, G. Deo, Effects of modifying  $\text{Ni}/\text{Al}_2\text{O}_3$  catalyst with cobalt on the reforming of  $\text{CH}_4$  with  $\text{CO}_2$  and cracking of  $\text{CH}_4$  reaction, *Int. J. Hydrog. Energy* 39 (2014) 11462–11472, <https://doi.org/10.1016/j.ijhydene.2014.05.058>.

[43] L. Ye, M. Zhang, P. Huang, G. Guo, M. Hong, C. Li, J.T.S. Irvine, K. Xie, Enhancing  $\text{CO}_2$  electrolysis through synergistic control of non-stoichiometry and doping to tune cathode surface structures, *Nat. Commun.* 8 (2018) 14785, <https://doi.org/10.1038/ncomms14785>.

[44] X. Zhang, Y. Song, F. Guan, Y. Zhou, H. Lv, Q. Liu, G. Wang, X. Bao,  $(\text{La}_{0.75}\text{Sr}_{0.25})_{0.95}(\text{Cr}_{0.5}\text{Mn}_{0.5})\text{O}_{3-\delta}\text{Ce}_{0.8}\text{Gd}_{0.2}\text{O}_{1.9}$  scaffold; old composite cathode for high temperature  $\text{CO}_2$  electroreduction in solid oxide electrolysis cell, *J. Power Sources* 400 (2018) 104–113, <https://doi.org/10.1016/j.jpowsour.2018.008.017>.

[45] S. Bernal, J.A. Diaz, R. Garcia, J.M. Rodriguez-Izquierdo, Study of some aspects of the reactivity of  $\text{La}_2\text{O}_3$  with  $\text{CO}_2$  and  $\text{H}_2\text{O}$ , *J. Mater. Sci.* 20 (1985) 537–541, <https://doi.org/10.1007/BF01026524>.

[46] T.H. Shin, J.H. Myung, M. Verbraeken, G. Kim, J.T.S. Irvine, Oxygen deficient layered double perovskite as an active cathode for  $\text{CO}_2$  electrolysis using a solid oxide conductor, *Faraday Discuss.* 182 (2015) 227–239, <https://doi.org/10.1039/c5fd0025d>.

[47] Y.S. Chung, H. Kim, H.C. Yoon, J.S. Chung, N.M. Sammes, Effects of manganese oxide addition on coking behavior of  $\text{Ni}/\text{YSZ}$  anodes for SOFCs, *Fuel Cells Weinheim (Wein)* 15 (2015) 416–426, <https://doi.org/10.1002/fuce.201400166>.

[48] Y. Cheng, C. Xu, L. Jia, J.D. Gale, L. Zhang, C. Liu, P.K. Shen, S.P. Jiang, Pristine carbon nanotubes as non-metal electrocatalysts for oxygen evolution reaction of water splitting, *Appl. Catal. B: Environ.* 163 (2015) 96–104, <https://doi.org/10.1016/j.apcatb.2014.07.049>.

[49] B.S. Yeo, A.T. Bell, Enhanced activity of gold-supported cobalt oxide for the electrochemical evolution of oxygen, *J. Am. Chem. Soc.* 133 (2011) 5587–5593, <https://doi.org/10.1021/ja200559j>.

[50] A. Wolfbeisser, O. Sophiphun, J. Bernardi, J. Wittayakun, K. Föttinger, G. Rupprecht, Methane dry reforming over ceria-zirconia supported Ni catalysts, *Catal. Today* 277 (2016) 234–245, <https://doi.org/10.1016/j.cattod.2016.04.025>.

[51] K. Takanabe, K. Nagaoka, K. Nariai, K. Aika, Titania-supported cobalt and nickel bimetallic catalysts for carbon dioxide reforming of methane, *J. Catal.* 232 (2015) 268–275, <https://doi.org/10.1016/j.jcat.2005.03.011>.

[52] B. Yan, Q. Wu, J. Cen, J. Timoshenko, A.I. Frenkel, D. Su, X. Chen, J.B. Parise, E. Stach, A. Orlov, J.G. Chen, Highly active subnanometer Rh clusters derived from Rh-doped  $\text{SrTiO}_3$  for  $\text{CO}_2$  reduction, *Appl. Catal. B: Environ.* 237 (2018) 1003–1011, <https://doi.org/10.1016/j.apcatb.2018.06.074>.

[53] Z. Geng, Y. Cao, W. Chen, X. Kong, Y. Liu, T. Yao, Regulating the coordination environment of Co single atoms for achieving efficient electrocatalytic activity in  $\text{CO}_2$  reduction, *Appl. Catal. B: Environ.* 240 (2019) 234–240, <https://doi.org/10.1016/j.apcatb.2018.08.075>.

[54] D. Neagu, T. Oh, D.N. Miller, H. Menard, S.M. Bukhari, S.R. Gamble, R.J. Gorte, J.M. Vohs, J.T.S. Irvine, Nano-socketed nickel particles with enhanced coking resistance grown in situ by redox exsolution, *Nat. Commun.* 6 (2015) 8120, <https://doi.org/10.1038/ncomms9120>.

[55] J. Chen, A. Bertei, E. Ruiz-Trejo, A. Atkinson, N.P. Brandon, Characterization of degradation in nickel impregnated Scandia-stabilized zirconia electrodes during isothermal annealing, *J. Electrochem. Soc.* 164 (2017) F935–F943, <https://doi.org/10.1149/2.0821709jes>.